Structural Engineering and Mechanics, Vol. 3, No. 6 (1995) 529-539
DOI: http://dx.doi.org/10.12989/sem.1995.3.6.529

Automated yield-line analysis of beam-slab systems

David Johnson †

Department of Civil and Structural Engineering, The Nottingham Trent University, Nottingham NG1 4BU, U.K.

Abstract. The rigid-plastic yield-line analysis of isotropically reinforced concrete slabs acting in conjunction with torsionally weak supporting beams is developed as the lower-bound form of a linear programming formulation. The analysis is extended to consider geometric variation of chosen yield-line patterns by the technique of sequential linear programming. A strategy is followed of using a fine potential yield-line mesh to identify possible collapse modes, followed by analysis using a coarser, simplified mesh to refine the investigation and for use in conjunction with geometric optimization of the yield-line system. The method is shown to be effective for the analysis of three slabs of varying complexity. The modes detected by the fine and simplified analyses are not always similar but close agreement in load factors has been consistently obtained.

Key words: reinforced concrete; slab-beam systems; automated yield-line analysis; sequential linear programming

1. Introduction

The author's previous work on the automated yield-line analysis of reinforced concrete slabs (Johnson 1995) has extended a linear programming formulation, originally proposed by Anderhaggen and Knopfel (1975), to allow for the geometric variation of a proposed yield-line pattern, so that its optimum geometry can be determined. The geometric optimisation was formulated as a sequential linear programming problem by linearising the effects of geometrical variation at any individual iteration. This approach proved convenient, since it made repeated use of the linear programming solution, which was central to the basic automated yield-line algorithm.

The problem of determining the critical collapse mode *ab initio* has also been examined (Johnson 1994). The approach recommended in this instance was to use a fine 'finite element' type (Fig. 1b) of triangulated mesh initially to provide a variety of positions and directions along which yielding can potentially occur. This net is analysed without geometric optimisation (which would be too complex in such a case) in order to establish the likely collapse mode. Based on the results of the fine net analysis, a simplified triangulation is devised which is suitable for geometric optimisation and which is capable of modelling the expected form of collapse (Fig. 1c, for example).

The work reported so far has been based on the assumption of rigid edge supports and the intention of the present paper is to extend the formulation to flexible boundary conditions in the form of edge beams. Consistent with the rigid-plastic behavioural model adopted for the slab response, the beams are also presumed to be rigid until an ultimate moment of resistance M is attained, at which stage a plastic hinge is formed and rotation may occur without further increase in moment. Beams are further assumed to be perfectly flexible in torsion.

† Principal Lecturer

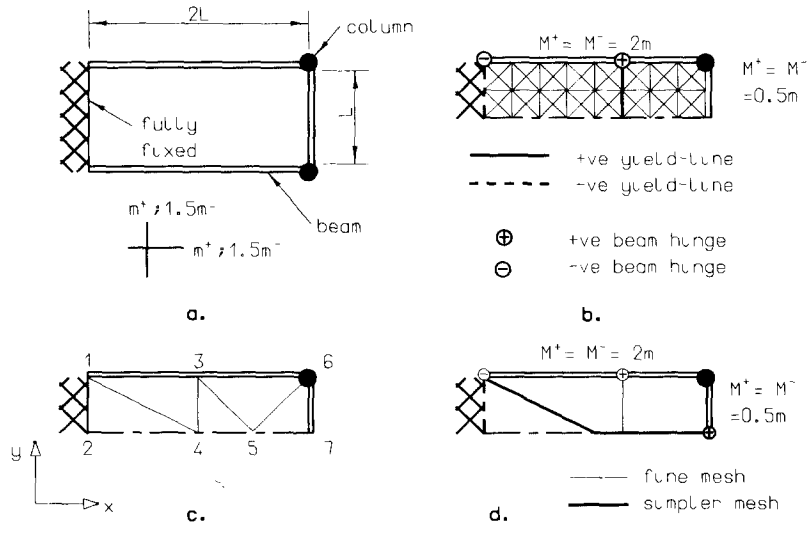

Fig. 1 a. Propped cantilever slab; b. yield-line system for half-slab. c. simplified mesh; d. yield-line system for simplified mesh.

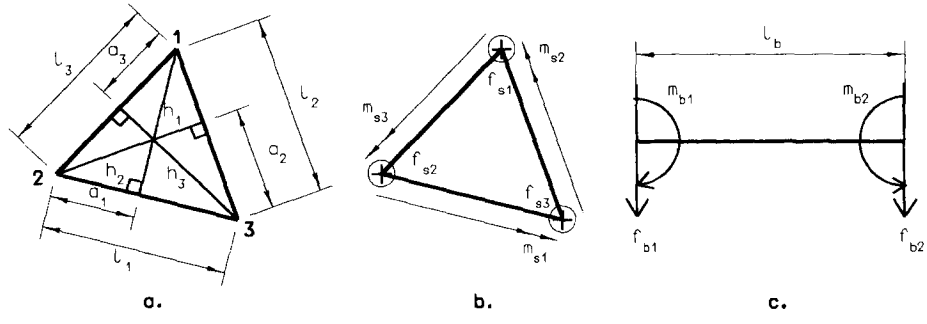

Fig. 2 a. Triangular region; b. statics of region; c. statics of beam element.

2. Theory

The slab to be analysed is meshed into triangular regions, a typical such region being shown in Fig. 2a. In Fig. 2b, the slab moments/per unit length m_{s1}, m_{s2}, m_{s3} are assumed uniform along the edges of the triangle. These moments are further assumed to be in equilibrium with nodal vertical forces f_{s1}, f_{s2}, f_{s3}, so that by statical considerations:

$$\boldsymbol{C}_s^e \boldsymbol{m}^e = \boldsymbol{f}_s^e \tag{1}$$

where $\boldsymbol{m}_s^e = \{m_{s1}, m_{s2}, m_{s3}\}^t$, $\boldsymbol{f}_s^e = \{f_{s1}, f_{s2}, f_{s3}\}^t$ and

$$\boldsymbol{C}_s^e = \begin{bmatrix} -\left(\frac{a_1}{h_1}+\frac{a_2}{h_2}\right) & \frac{a_2}{h_2} & \frac{a_1}{h_1} \\ \frac{a_2}{h_2} & -\left(\frac{a_2}{h_2}+\frac{a_3}{h_3}\right) & \frac{a_3}{h_3} \\ \frac{a_1}{h_1} & \frac{a_3}{h_3} & -\left(\frac{a_3}{h_3}+\frac{a_1}{h_1}\right) \end{bmatrix}$$

in which $a_1=\frac{l_1^2-l_2^2+l_3^2}{2l_1}$ and $h_1=\frac{(y_1-y_2)(x_3-x_2)-(x_1-x_2)(y_3-y_2)}{l_1}$. (other values of a, h are obtained by cyclic suffix permutation).

If beams are included in the formulation, then similar equilibrium considerations need to be applied to relate the contributions to the nodal forces arising from beam moments. Thus, if the moments at the ends of a beam segment are m_{b1} and m_{b2} (Fig. 2c), then the end forces f_{b1} and f_{b2} may be related to the beam end moments by equilibrium considerations such that:

$$\boldsymbol{C}_b^e \boldsymbol{m}_b^e = \boldsymbol{f}_b^e \tag{2}$$

where $\boldsymbol{m}_b^e=\{m_{b1}, m_{b2}\}^t$, $\boldsymbol{f}_b^e=\{f_{b1}, f_{b2}\}^t$ and $\boldsymbol{C}_b^e=\frac{1}{l_b}\begin{bmatrix}1 & -1\\ -1 & 1\end{bmatrix}$

Summing contributions from all the *ne* regions and *nbe* beams to the forces at all the *nj* nodes. due to the moments along the total number of boundaries *nb* and at the total number of distinct beam end positions *nbep* gives the complete set of equilibrium conditions:

$$\boldsymbol{C}\boldsymbol{m}=\boldsymbol{f} \tag{3}$$

where $\boldsymbol{m}=\{m_{s1}, \cdots, m_{snb}, m_{b1}, \cdots, m_{bnbep}\}^t=\{\boldsymbol{m}_s, \boldsymbol{m}_b\}^t$ and $\boldsymbol{f}=\{f_1, \cdots, f_{nj}\}^t$

To account for the imposed boundary conditions, it should be noted that, in forming Eq. (3), equilibrium equations are not formed at nodes which are restrained against vertical displacement and moment variables are not included in respect of zero moment (free or simply supported) edge boundaries or zero moment beam ends (simple supports).

Under isotropic conditions, all the moments/unit length will be bounded by the constant plastic moments of resistance/unit length in positive and negative bending m^+ and m^-, respectively, such that:

$$\boldsymbol{u}m^- <= \boldsymbol{m}_s <= \boldsymbol{u}m^+ \tag{4}$$

where $\boldsymbol{u}=\{1, \cdots, 1\}^t$ is the unit vector.

Furthermore, the beam moments $\boldsymbol{m}_b$ will be limited such that:

$$\boldsymbol{M}^- <= \boldsymbol{m}_b <= \boldsymbol{M}^+ \tag{5}$$

In Eq. (5), $\boldsymbol{M}^+$, $\boldsymbol{M}^-$ are the vectors of ultimate moments of resistance in positive and negative bending, respectively, of the beam sections at the distinct beam positions.

In the interests of simplicity, uniform loading conditions will be presumed. Under the action of a uniform load of intensity q the statically equivalent nodal forces for a typical triangular element (Fig. 2a) are given by:

$$\boldsymbol{f}_q^e=\left\{\frac{q\Delta}{3}, \frac{q\Delta}{3}, \frac{q\Delta}{3}\right\}^t \tag{6}$$

where $\Delta=\frac{h_1 l_1}{2}$

Summing nodal loading contributions of the form given by Eq. (6), results in a set of total nodal loads $\boldsymbol{f}_q$ which are statically equivalent to the nodal loads $\boldsymbol{f}$ which were ((Eq. (3)) derived from equilibrium slab and beam moment considerations. Thus, at a load factor λ the final

equilibrium equations becomes:

$$\boldsymbol{C}\boldsymbol{m}=\lambda \boldsymbol{f}_q \tag{7}$$

Eqs. (7) and (4-5) represent the conditions of equilibrium and yield, respectively, for the slab. By the lower bound theorem of plasticity, the collapse solution may therefore be obtained by maximising the load factor λ subject to the linear conditions expressed by the above equations. This is a linear programming problem and may be solved by standard techniques (see Garvin 1960).

2.1. Displacement and rotation solution

The linear programming solution will provide the collapse load factor and the slab boundary and beam moment values at collapse. To obtain the yield-line pattern at collapse, it is necessary to determine the rotations along the specified boundaries and at the beam nodal positions, since only boundaries and beam nodal positions with non-zero rotations will represent yield-lines and beam hinges, respectively. Boundary rotations, θ, and nodal displacements $\boldsymbol{w}$ may be conveniently determined by application of the 'dual' properties of linear programming (see Munro and Da Fonseca 1978 and Garvin 1960).

2.2. Variable yield-line geometry

If variation in yield-line geometry is considered, then Eq. (7) becomes non-linear since both $\boldsymbol{C}$ and $\boldsymbol{f}_q$ are geometry dependent. The technique of sequential linear programming relies on an iterative process in which linearised approximations are used in any particular iterations, Eq. (7) may be linearised by replacing each term by its first-order Taylor series approximation to give:

$$\dot{\boldsymbol{C}}\boldsymbol{m}+\dot{\boldsymbol{J}}_{Cx}\boldsymbol{\Delta}_x=\lambda\dot{\boldsymbol{f}}_q+\lambda\dot{\boldsymbol{J}}_{fx}\boldsymbol{\Delta}_x \tag{8}$$

where $\boldsymbol{\Delta}_x=\boldsymbol{x}-\dot{\boldsymbol{x}}$ and $\boldsymbol{x}$ is the geometric variable vector.

In Eq. (8), $\cdot$ indicates evaluation with respect to the current geometry, and such terms therefore, remain constant during the succeeding iteration. Also, the Jacobian matrices $\dot{\boldsymbol{J}}_{Cx}$ and $\dot{\boldsymbol{J}}_{fx}$ are given by:

$$\dot{\boldsymbol{J}}_{Cx}=\left[\cdots, \frac{\partial \dot{\boldsymbol{C}}}{\partial x_i}\dot{\boldsymbol{m}}, \cdots\right] \text{ and } \dot{\boldsymbol{J}}_{fx}=\left[\cdots, \frac{\partial \dot{\boldsymbol{f}}_q}{\partial x_i}, \cdots\right] \tag{9}$$

The derivatives required for the construction of the Jacobian matrices of Eq. (9) may be obtained analytically and appropriate expressions have been provided previously for the pure slab situation (Johnson 1995). In the case of beam-slab systems, the same Jacobian matrices have been utilised on the assumption that movement of beam hinge positions is a secondary feature which will not significantly affect the iterative procedure. Appropriate contributions to the relevant Jacobian matrix, due to variation in the beam hinge positions, could, however, be incorporated if so desired.

The previous equilibrium constraints, Eq. (7), are replaced by Eq. (8) and the linear programming solution is repeated. At the conclusion of the programming procedure, the 'objective function' values corresponding to the geometric variables $\boldsymbol{\Delta}_x$ will indicate the sense in which the variables need to be amended in order to appropriately modify the load factor. At this stage, reductions in the load factor are sought since geometric variation represents an upper-bounded

solution.

2.3. Bounds on geometric variations and convergence

The magnitudes of the changes to the geometric variables cannot be obtained from a linear solution and must be enforced by the imposition of suitable bounds. Clearly, the geometric variables will need to be constrained by lower bounds $\underline{\tilde{x}}$ and upper bounds $\bar{\tilde{x}}$ which are designed to ensure that the confines of the slab and its basic topology are not altered. In addition, however, geometric variation at any iteration must be limited so that unacceptable linearization errors do not occur. The errors incurred by geometric linearization have been taken to be dependent on the fineness of the local triangulation, on the premise that the linearization will remain effective if all amendments to the areas of the triangular regions and the orientations of the boundaries remain within a specified tolerance. Thus, if, for all the boundaries meeting at node i, the average, absolute value of the projection of the triangle edges in respect of geometric variable x_i is $\tilde{x}_i$ then the bounds are given by:

$$max(\underline{\tilde{x}},\ \lceil(1-\beta_i)\rfloor\tilde{x})<=x<=min(\bar{\tilde{x}},\ \lceil(1+\beta_i)\rfloor\tilde{x}) \tag{10}$$

where $\lceil(1\pm\beta_i)\rfloor$ are the diagonal *move limit* matrices.

All the individual move limits β_i are initially taken to be 0.25 to allow reasonable geometric change but not so as to produce undue distortion of the sub-division. Subsequently, the move limits are expanded such that $\beta_i=1.1\ \beta_i$ if the three previous iterations indicate a consistent direction of variation in a given parameter. If the three previous iterations indicate an oscillation in a parameter, this is taken as indication that a critical value has been passed and the bounds are tightened by setting $\beta_i=0.5\ \beta_i$ so that the solution is driven towards the critical value.

Convergence of the sequential linear programming process is based on successive changes in load factor. A stipulation that none of the latest three load factor values vary by more than 0.1% has generally been found to be effective in ensuring reasonable accuracy, and in preventing accidental termination due to coincidentally similar successive values.

3. Examples

In the following examples, uniform loading of intensity q and uniform, isotropic top and bottom reinforcement have been assumed for simplicity throughout. The ultimate moment capacities of supporting beams M have been expressed, numerically, as multiples of the characteristic slab moment of resistance m. In the first two examples, the ultimate loads have been determined in terms of a load factor λ and a characteristic dimension L, such that $q_u=\lambda m/L^2$. In the final example, the ultimate load has been determined in terms of a load factor λ, such that $q_u=\lambda m$. A load factor which is subscripted as $\ddot{\lambda}$ indicates that the value has been obtained as the result of a converged geometrical optimization process. Point and line loading, or variable, orthotropic reinforcement obviously complicate the procedures used, but do not, in principle, pose insuperable obstacles.

3.1. Propped cantilever slab

The rectangular, uniform slab shown in Fig. 1a is fully fixed at its left-hand side and propped by columns at its right-hand corners. The three unrestrained sides are supported on beams

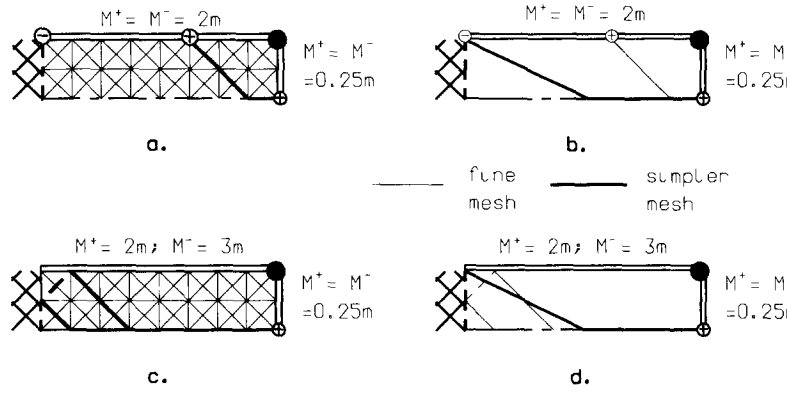

Fig. 3 Propped cantilever slab
a. *fe* collapse mode ($M=2m$, $0.25m$); b. *s* collapse mode ($M^+=2m$, $0.25m$)
c. *fe* collapse mode ($M^+=2m$, $0.25m$, $M^-=3m$, $0.25m$); d. *s* collapse mode ($M^+=2m$, $0.25m$, $M^-=3m$, $0.25m$)

of flexural capacity $M^{\pm}=2m$ along the longer sides and $M^{\pm}=0.5m$ along the shorter side. The columns are presumed to offer point support only and to be adequately reinforced against local failure. Making use of symmetry and adopting the fine 'finite-element' type of mesh shown in Fig. 1b, the 'propped cantilever' form of collapse shown in Fig. 1b is predicted at a load factor $\lambda=15.1$. A further analysis has been undertaken, using the simplified mesh shown in Fig. 1c. For this mesh, geometrical optimisation was performed, using x_3, x_4 and x_5 as the geometric variables, with a 'linkage' (Johnson 1995) being enforced such that $x_4=x_3$. The yield-line pattern at collapse obtained from this analysis is quite different (Fig. 1d). A Y-type collapse mode is predicted, which is characteristic of slabs supported on three sides only. Despite the distinct collapse mode, there is little change in load factor, the value determined by the simplified mesh being $\ddot{\lambda}=15.0$.

Previous investigations (Johnson 1994) have shown that finite element type meshes generally do give reasonable indications of collapse modes in pure slab situations. Clearly, this is less likely if competing mechanisms exist at similar load factors. Once edge beam collapse is introduced into the system, the number of potential modes increases significantly and the likelihood of competing modes existing at virtually the same load factor similarly increases. It might be expected, therefore, that situations such as that experienced in the present example will occur reasonably regularly.

To examine the finite element/simplified mesh comparison further, the shorter edge beam capacity was reduced to $M^{\pm}=0.25\ m$ (Fig. 3a). The results for the finite element and the simplified meshes are shown in Figs. 3a and 3b, respectively. It may be seen that the modes still differ, although the finite element meshing has produced a combined 'Y' and propped cantilever mode, which now incorporates a hinge in the weakened end beam. The simplified mesh continues to suggest a Y type mode at a load factor, $\ddot{\lambda}=13.8$, which shows a slightly more pronounced reduction on the finite element mesh value ($\lambda=14.5$) than in the previous case.

Finally, to encourage both meshes to avoid hinge formation in the longer edge beams, the negative bending capacity of these members was raised to $M^-=3m$. The finite element (*fe*) mesh mode is now a modified Y type (Fig. 3c) and does bear some resemblance to the simplified (*s*) mesh result (Fig. 3d). The relevant load factors are $\lambda=15.0$ (*fe*) and $\ddot{\lambda}=13.8$ (*s*) (unchanged from the previous analysis since negative hinges in the longer edge beams are not involved).

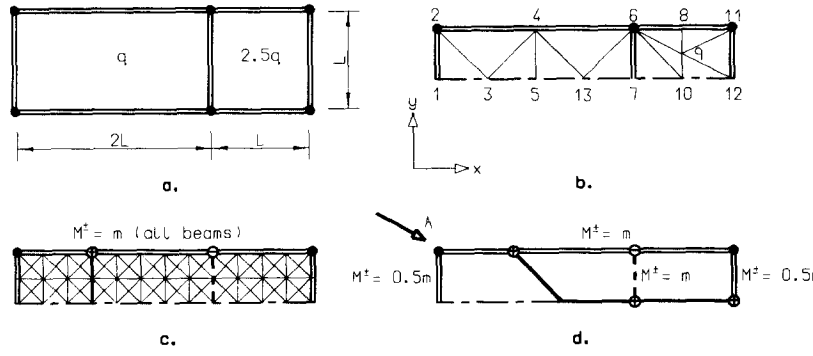

Fig. 4 a. Two-bay slab; b. simplified mesh; c. *fe* collapse mode; d. *s*. collapse mode.

Thus, rather similar modes have given rise to an enhanced load factor variation. This is probably a vagary of the modelling employed, however, and the difference of 9% is distinct but not large. The *fe* mode does resemble 'corner lever' (Wood 1961) action, but care is needed in drawing such a conclusion. In some cases, diagonal negative yield-lines in corners may be indicative of a corner lever. In others, however, it can be symptomatic of the inability of a *fe* mesh to accurately model the geometry of the collapse system (Fig. 3c) and therefore be a feature of the meshing rather than a manifestation of a physical property of the collapse mode. In the present case, the *fe* mesh does not allow a sagging diagonal yield-line to propagate from the restrained corner of the slab close to the geometry suggested by the simplified analysis. The function of the diagonal negative yield-line is therefore to allow a positive line to form in the vicinity of the simplified mode line (Fig. 3d).

3.2. Two-bay beam slab system

The two-bay system shown in Fig. 4a consists of uniform, isotropic slabs supported by edge beams. The smaller, right-hand bay supports a uniformly distributed load which has two and a half times the intensity of the load carried by the larger, left-hand bay. The system has again been analysed by both a *fe* type mesh (Fig. 4c) and a simplified mesh (Fig. 4b). For the purposes of geometric iteration, the geometric variables were taken to be x_3, $x_4(=x_5)$, $x_9(=x_8=x_{10})$, x_{13} and y_9.

If the edge beams are presumed to possess ultimate moments of resistance which are numerically equal to that of the slabs, then both analyses indicate the 'propped cantilever' mode of collapse shown in Fig. 4c. The relevant load factors are $\lambda=8.80$ (*fe*) and $\ddot{\lambda}=8.79$ for the simplified (*s*) mesh. On reducing the moments of resistance of the edge transverse beams to $M^{\pm}=0.5m$, however, the load factors drop slightly to $\lambda=8.52$ (*fe*) and $\ddot{\lambda}=8.49$ (*s*). The mode predicted by both analyses is quite different to the first case (Fig. 4d) and involves the collapse of both bays (Fig. 5). Clearly it is difficult to anticipate a mode such as shown in Fig. 5 and, for the construction of appropriate simplified meshes, it is necessary to rely on trial-and-error and on the results provided by *fe* type meshes.

If the beams are strengthened relative to the slab, as shown in Fig. 6a, then yet a further mode is encountered -in this case a 'Y' type mode involving both bays and two of the transverse beams- at a load factor of $\lambda=10.2$. Further strengthening of the central transverse beam results in the Y mode being restricted to the smaller span (Fig. 6) and increases the load factor to

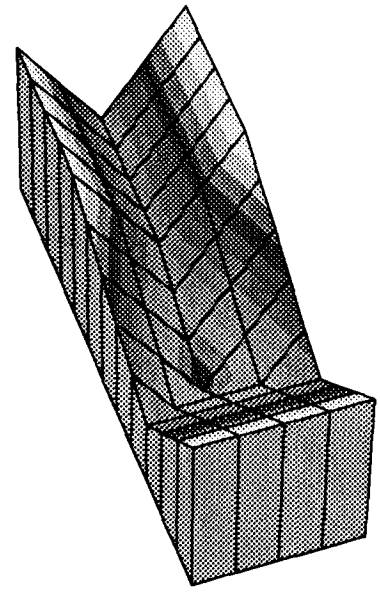

Fig. 5 Two-bay slab: isometric view of collapse mode in view direction A of Fig. 4d.

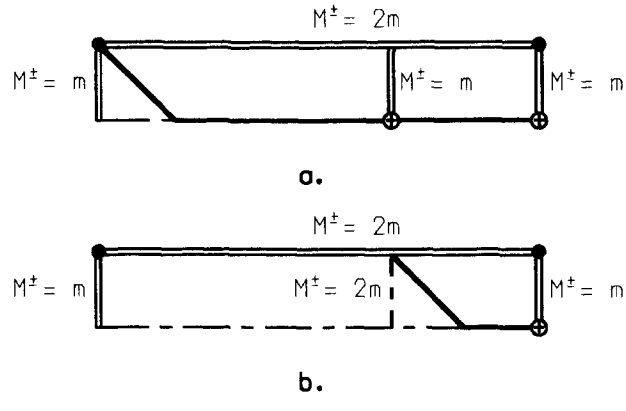

Fig. 6 a. *fe* collapse mode; b. *s* collapse mode.

$\lambda = 11.5$. In both these cases, there is good agreement between the *fe* and *s* type mesh solutions. It has also been shown that further increase in the capacity of the outer two transverse beams to $M^{\pm} = 2m$ results in a pure slab collapse mode, which occurs in the left-hand bay at a load factor of $\ddot{\lambda} = 15.8$.

3.3. Interconnected beam-slab system

The beam-slab system shown in Fig. 7a is a adaptation of an interconnected slab arrangement previously considered by Munro and Da Fonseca (1978) in which supporting beams are employed

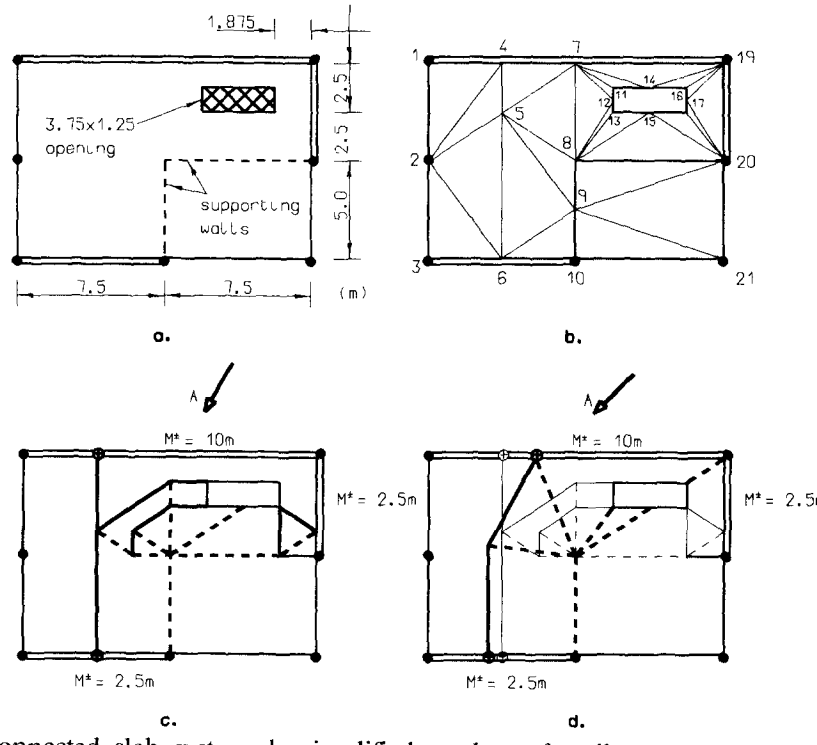

Fig. 7 a. Interconnected slab system; b. simplified mesh; c. *fe* collapse mode; d. *s* collapse mode.

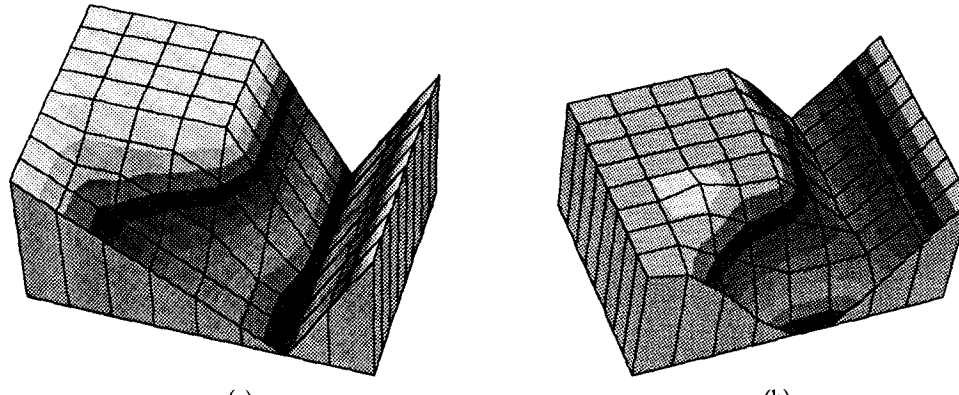

Fig. 8 Isometric views of interconnected slab collapse modes
a. *fe* mode in view direction A of Fig. 7c; b. *s* mode in view direction A of Fig. 7d.

in place of the original simple edge supports. Predicting a likely critical yield-line pattern for such a complex system is virtually impossible and guidance from a *fe* mesh solution is essential before attempting to construct a simpler meshing for geometric optimisation purposes. For the beam capacities indicated, Fig. 7c shows the mode predicted by an *fe* mesh based on $1.875 \times 1.25m$ modules. The collapse mode is difficult to categorize simply but clearly incorporates a propped cantilever mode in the largest, left-hand slab. This feature continues into the upper, right-hand

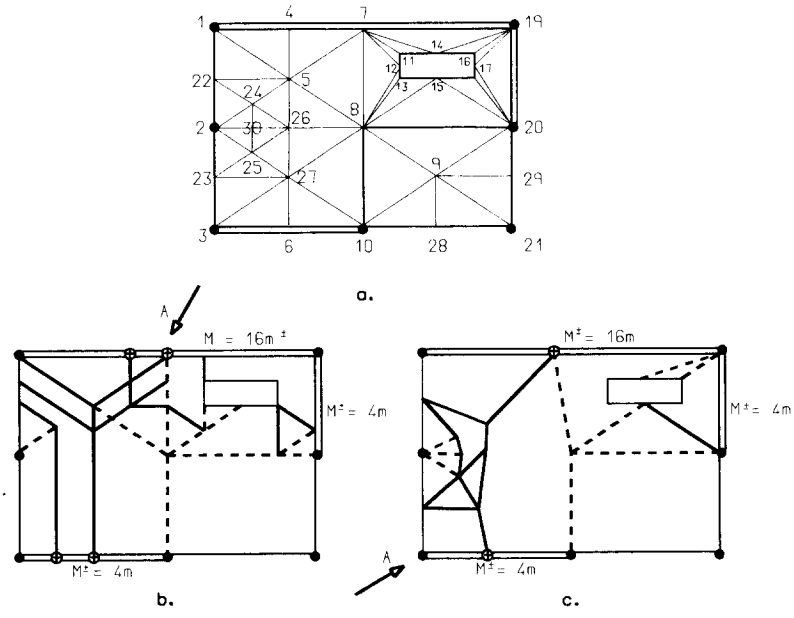

Fig. 9 Interconnected slab system with strengthened beams
a. modified simple mesh; b. *fe* mode: c. *s* mode.

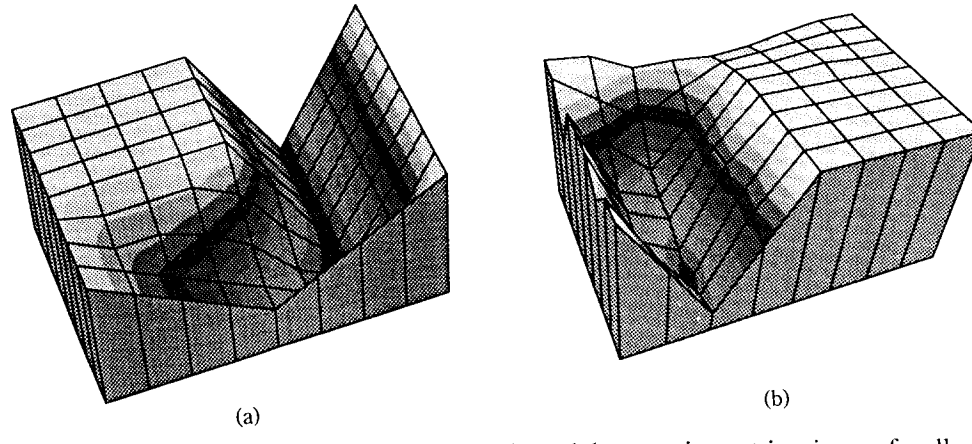

Fig. 10 Interconnected slab system with strengthened beams: isometric views of collapse modes
a. *fe* mode in view direction A of Fig. 9b; b. *s* mode in view direction A of Fig. 9c.

slab by means of a 'fan' type system (Wood 1961) centred on the corner of the internal beam supports. Collapse was at a load factor $\lambda=0.312$, which is a 22% reduction on the pure slab value of $\lambda=0.40$ calculated by Munro and Da Fonseca.

Based on this solution, the simplified mesh shown in Fig. 7b was adopted. For the purpose of geometric optimization, variations in $x_4(=x_5=x_6)$, x_7, x_{14}, x_{15}, y_5, y_9, y_{12}, y_{17} were allowed. The resulting solution is illustrated in Fig. 7d, where it is compared with the *fe* solution (fine lines). The simplified mesh solution confirms the presence of the fan system, an indication of which may also be gained from the isometric views of the collapse modes provided in Fig. 8. The load factor achieved by this simpler mesh was $\lambda=0.304$, which was only a slight (3%)

reduction on the *fe* value.

If the beam capacities are enhanced to the values shown in Fig. 9 then the *fe* solution gives a load factor of $\lambda=0.367$. The relevant collapse mode is shown in Fig. 9b and it may be seen that the mode is now of a Y form. Also, there is some evidence of collapse around the central column along the left-hand slab edge, which is the pure slab mode (Munro and Da Fonseca 1978). To incorporate this latter possibility, it was necessary to extend the simplified meshing to the form shown in Fig. 9a, for which the geometric variables were taken to be x_4, x_5, x_6, x_7, x_9, x_{14}, x_{15}, x_{24}, x_{25}, x_{26}, x_{28}, x_{30} and y_5, y_9, y_{12}, y_{17}, y_{22}, y_{23}, y_{24}, y_{25}, y_{29}, y_{30}. The resulting mode (Fig. 9c) shows enhanced collapse around the central left-hand side column and less participation of the upper right-hand slab portion. The basic Y type system remains however, as may be verified from the comparative isometric plots (Fig. 10). Once again the load factor achieved by the simplified mesh ($\lambda=0.355$) was only 3% less than the *fe* value.

4. Conclusions

(1) The use of sequential linear programming together with a strategy of initial use of a fine (*fe*) meshing verified by a simplified (*s*) mesh provides a systematic and robust procedure whereby mechanisms and load factors for beam-slab yield-line collapse may be determined.

(2) Since beam-slab systems commonly exhibit a multiplicity of potential yield-line mechanisms, the probability of two or more different mechanisms having similar load factors is greater than for pure slabs. There is therefore an increased likelihood of a *fe* mesh producing a different mechanism to that derived from a simplified mesh. It also follows that more care is needed in the construction of simplified meshes since mechanism possibilities other than those directly suggested by the *fe* solution need to be considered. A certain degree of trial-and-error may be required.

(3) *Fe* collapse mode solutions may be complex and possibly present difficulties of interpretation if the selected mesh does not allow the accurate representation of the critical mechanism. Rerunning with a varied mesh density and/or proportioning can be helpful in such cases.

(4) In the examples considered, differences in load factor between *fe* and *s* based mesh solutions did not exceed 10%, although quite different mechanisms could be involved. Furthermore, the reductions in load factors produced by geometrical optimisation were also modest-again less than 10%.

References

Anderhaggen, E. and Knopfel, H. (1975), "Berechnung der Traglast von Stahlbetonplatten Mittels Finiter Elemente", *Schweizerische Bauzeitung*, **93**(20), 313-316.

Dickens, J.G. and Jones, L.L. (1988), "A general computer program for the yield-line solution of edge supported slabs", *Computers and Structures*, **30**(3), 465-476.

Garvin, W.W. (1960), *Introduction to linear programming*, McGraw-Hill, New York.

Johnson, D. (1995), "Yield-line analysis by sequential linear programming", *International Journal of Solids and Structures*, **32**(10), 1395-1404.

Johnson, D. (1994), "Mechanism determination by automated yield-line analysis", *The Structural Engineer*, **72**(19), 323-327.

Munro, J. and Da Fonseca, A.M.A. (1978), "Yield-line method by finite elements and linear programming", *The Structural Engineer*, **56B**(2), June, 37-44.

Wood, R.H. (1961), *Plastic and elastic design of slabs and plates*, Thames and Hudson, London.